Ceramics International 45 (2019) 16829–16835

Contents lists available at ScienceDirect

Ceramics International

journal homepage: www.elsevier.com/locate/ceramint

A study on 3D graphene synthesized directly on Glass/FTO substrates: Its Raman mapping and optical properties

Ozkan Bayram[a,b,*]

[a] Bayburt University, Engineering Faculty, Department of Electrical and Eelectronics Engineering TR-69100, Bayburt, Turkey
[b] Ataturk University, Graduate School of Natural and Applied Sciences, Department of Nanoscience and Nanoengineering, TR-25240, Erzurum, Turkey

ARTICLE INFO

Keywords:
VGN
Raman mapping
PECVD
Non-catalyst surfaces
CH_4

ABSTRACT

In this study, vertically oriented (3D) graphene nanostructures (VGN) were obtained on Glass and Fluorine doped tin oxide (FTO) substrates at relatively low temperatures (approaximatelly at 400 °C) by using plasma enhanced chemical vapor deposition (PECVD) technique. VGNs were characterized using Raman, Uv–Vis and SEM spectroscopies, respectively. Raman spectroscopy showed that growth temperature significantly affected VGN formation and film quality. The layer structures of these VGNs were also confirmed by Raman mapping. The most important data obtained from this study is that although the applied radio frequency (RF) power is the same, the growth temperature significantly affects the graphene formation and morphologies. This was attributed to the fact that CH_4 decomposition was very difficult at low temperatures. The optical transmittance of VGNs ranged from 50% to 95% (at 550 nm wavelength) and their electrical conductivity was also determined to be between 5.94 kohm/sqr and 11.2 kohm/sqr. The electrical and optical properties of VGNs, which have a large surface area, indicated that they may be an alternative material for sensor, solar cell and supercapacitor applications.

1. Introduction

Grafen, one of the most important two-dimensional (2D) materials, has been extensively researched for possible applications since the last 10 years due to its superior structural and electrical properties [1–5]. Some of these studies focused on the graphene growth mechanisms, but some of them have turned to its current applications due to their superior electronic and optical properties. Although there are not many studies about the growth mechanism of graphene, a lot of studies have been carried out for possible applications. Due to its high specific surface area high carrier mobility, superior optical transmittance and carrier concentration, it has been highly tested in graphene, supercapacitor and solar cell applications. For example, monolayer graphene has a high carrier mobility ($> 200\,000\ cm^{-2} V- 1 s^{1}$ at an electron density of $4 \times 10^{9}\ cm^{-2}$), high specific surface area ($2600\ m^{-2} g^{-1}$), and high optical transparency (97.7%) [6,7]. All these advantages show that graphene, which is commonly used in dye-sensitized solar cells (DSSC), is a promising material for increasing the these cells efficiency [7–12]. In particularly, it has been used as a photoanode [13–16] and counter electrode [17–21] materials in DSSC applications. Because of its outstanding properties, Graphene, also attracts attention in sensor applicationssuch as biosensor [22–29], water sensors [30] and gas sensors [31–33]. In addition to the increasing of graphene applications, the fact that the growth process cannot be performed directly and transferred to another insulating substrate has a great effect on the quality and efficiency of these studies. Recently, a number of studies have been carried out for the production of vertical oriented graphene (VG) obtained on various metal catalysts at relatively high temperatures. However, this process could not eliminate the transfer problem in graphene applications. Possible wrinkles, holes and residues caused by etchant solution during the graphene transfer process have an important role on thin film quality. In order to avoid the negative effects of the transfer process, intensive efforts are being made to directly synthesize graphene on substrates such as FTO, ITO and soda-lime glass [34], which are widely used in solar cell applications. The optimum operating temperatures of these substrates are around 600 °C. Therefore, new techniques are required which enable to obtain graphene at relatively lower temperatures. The PECVD technique is a technique that makes this possible. Some researchers have reported that PECVD is a highly efficient method for the production of VGNs and allows the graphene to be obtained at low temperatures and directly without any catalyst [35–43]. The VGNs, which have unique electrical, chemical and mechanical properties compared to 2D graphene and which are obtained without the need for transfer operation, are now more

* Bayburt University, Department of Electrical and Electronics Engineering, Engineering Faculty, TR-69100, Bayburt, Turkey,
E-mail addresses: obayram@bayburt.edu.tr, ozkanbayram5555@hotmail.com.

https://doi.org/10.1016/j.ceramint.2019.05.224
Received 5 April 2019; Received in revised form 16 May 2019; Accepted 21 May 2019
Available online 22 May 2019
0272-8842/

promising for a wide variety of applications. For example, adjustable electrical conductivity and high specific surface area make VGNs an even more important material for supercapacitors, which are the current applications of 2D graphene [37,44–48]. In this study, it is aimed to obtain direct VGNs on material surfaces such as FTO and glass substrates which is one of the most important materials especially for DSSCs. FTO/graphene is used as the counter electrode material in these solar cells. The important thing is that graphene can be grown directly on FTO substrates to eliminate various defects that may occur during graphene transfer. In this study, it is aimed to produce graphene directly on these substrates by using PECVD technique in the temperature range of 400 ^{0}C-600 °C where the structural stability of FTO can be maintained. VGNs were analyzed using Raman, Raman mapping, SEM, Uv–Vis and I–V measurements.

2. Materials and method

2.1. Materials

The PECVD system used to obtain VGN nanostructures was established by the Nanovak (Ankara, Turkey) company. The CH_4 and H_2 gases used as precursor gas were obtained from Sigma Aldrich. To purify the substrates surfaces from foreign atoms, high purity Ar gas was used and this gas plasma was formed by the help of the RF generator and then the cleaning process was performed. On the other hand, alcohols such as ethanol, propanol and acetone used in surface cleaning of substrates were obtained by purchase from Tekkim (Ankara, Turkey) company. Glass and FTO materials were used as the substrate, and these materials were obtained from the commercially available Sigma Aldrich (Germany).

2.2. Growth of VGN by PECVD

The inductively coupled plasma (ICP) unit was adapted to the CVD technique commonly used in the graphene production process and the VGN structures are intended to be produced at relatively lower temperatures. Commercially purchased glass and FTO substrates were cut to the appropriate size and subjected to surface cleaning. Surface cleaning was carried out with the same procedure for each substrate. First, these substrates were washed with acetone, deionized (DI) water, propanol, DI water, ethanol and DI water, and finally rinsed. After completed treatment, each substrate was kept in vacuum environment. The PECVD system (Fig. 1. [49]) consists of a vacuum chamber, vacuum pump, heater, gas control units and RF power supply unit. After surface cleaning, each substrate was placed in the sample compartment of the PECVD system, respectively, and experimental studies were initiated. In the study, gas flow rates for CH_4 and Ar were determined as 10 sccm and 30 sccm, respectively. We can explain the stages of obtaining VGN structures on glass substrates as follows.

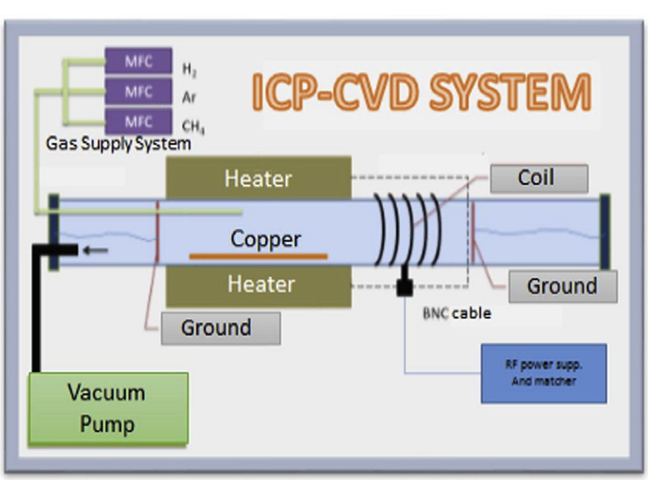

Fig. 1. Schematically represantation of PECVD system.

1. The pressure of the vacuum chamber is reduced to 10^{-4} mTorr using a vacuum pump.
2. Ar gas is sent to the vacuum environment by means of gas control unit and plasma is formed with the help of RF unit. This process is carried out for the surface cleaning of the substrates.
3. Using the heater, the temperature is set to the desired growth temperature. For FTO, this temperature was set at 480 °C, because the temperature at which the FTO could work without deterioration, ie without softening, is at approximately 480 °C. On the other hand, VGN structures were obtained at various temperature values for glass substrates. VGN production was performed at 600 °C(VGN1), 550 °C(VGN2), 500 °C(VGN3), 480 °C(VGN5) and 400 (VGN4) ^{0}C, respectively. Since glass substrate materials began to soften at about 620 °C, 600 °C was preferred as the highest temperature.
4. VGN Coatings were carried out for 30 min coating time and 100 W RF power. After the process was completed, the system was shut down and the next operation was started. The image of VGNs obtained at various growth temperatures and on different substrates was presented in Fig. 2.

3. Results and discussions

3.1. Growth mechanism of VGN

The structural defects caused by the transfer of graphene thin films grown on the metal catalyst to another well-formed insulated substrate significanly reduce the quality of this thin film. Alternative methods for possible graphene applications are being developed in order to eliminate these undesirable factors. Here, the PECVD technique plays an important role and allows for the directly growth of graphene at relatively lower temperatures and various substrates. In the PECVD environment, energetic electrons, free radicals and photons are generated at a high electric field and relatively low temperature [50]. For example, for methane (CH_4) precursor gas, CH_4 molecules are highly divided into various reactive species in this technique. These species are commonly known as CH_x +, C_2H_x +, C_3H_x +, C_4H_x +, CH, CH_2 and CH_3 [51,52]. The vertical orientation graphene film obtained under the PECVD process has a high specific surface area compared to 2D graphene, so it finds wide application in biosensors, both anode and cathode material in solar cells and supercapacitors. Here, the vertical orientation is also thought to be caused by the electric field in the PECVD system [53]. The basic steps of graphene growth on the glass surface are shown schematically as follows (Fig. 3a [54]). This figure shows that the plasma-enhanced chemical growth process creates a graphitic buffer layer on the glass surface. Later, due to possible lattice mismatch and dense ion bombardment between the glass substrate and the graphite carbon film, defects and curved areas on the surface occur [50]. The edges of the graphitic buffer layer cause vertical growth of the graphene by bending upwards due to the high electric field in the vacuum environment. The reasons for the graphene growth occuring in vertical oriented rather than two-diomensional (2D) graphene can be described as follows: due to the different chemical bonding nature, the defects caused by the interfacial tension between the glass substrate and the graphitic carbon are the most important factor of vertical orientation growth [53,54]. The surface tension effect causes the polycrystalline carbon buffer layer to form on the glass substrate. However, this buffer layer has curved orientations caused by defects. Another important factor is that the electric field in the PECVD technique has an important role in the growth and this electric field is applied in the vertical direction to the substrate surface. Thus, VGNs tend to grow in the same orientation as the electric field (Fig. 3b. [55]). Similarly, for the VGNs obtained on metal catalyst substrates such as copper, the most

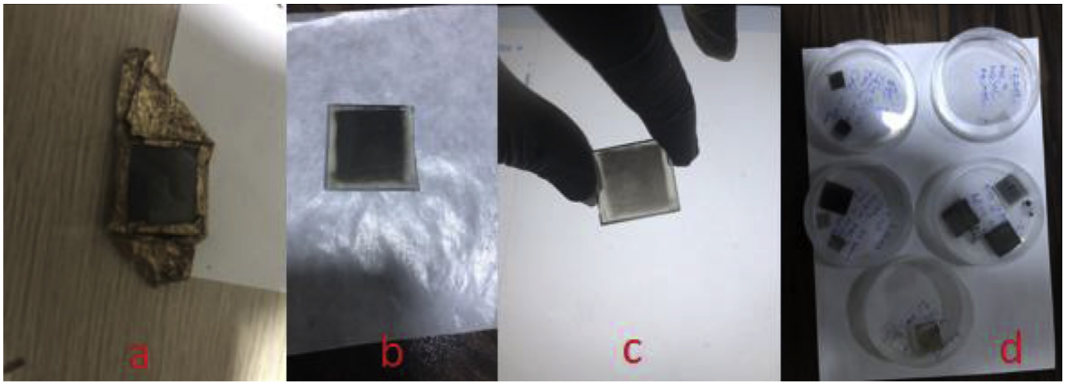

Fig. 2. Images of VGNs grown using the PECVD technique. a) FTO wrapped in copper foil material b) VGN grown on the FTO substrate c) VGN/FTO d) VGNs grown on glass substrates at various growth temperatures.

important factor is the electric field in the PECVD technique. The most basic similarity for both glass and metal catalyst substrates is the electric field used in the production technique.

3.2. Raman analyses of VGN

Figs. 4 and 5 show the Raman spectra of VGN samples prepared under different temperatures. As you can see from these graphs, The peaks D, G, and 2D of the VGN samples were determined at about 1348 cm^{-1}, 1588 cm^{-1} and 2698 cm^{-1}, respectively. The D peak, one of these peaks is attributed to the sp^3 hybrid construct resulting from crystal defects and irregular structures or to a sp^2 bond hybridization defect [56,57]. The other characteristic peak, the G-peak, is due to the stretching of the C-C bonds and is quite common for all sp^2 carbon system [58]. The 2D peak is due to the double-resonance Raman process in which two phonons of the opposite momentum are involved [59]. The ratios of the peak intensities ($I_D/I_G$and I_{2D}/I_G, respectively, from Figs. 3 and 4 were determined and are presented in Table 1. This table indicates that the I_D/I_G decreases from 2.64 to 2.01 with the growth temperature increase. The increase in growth temperature results in an increase of number of sp^3 hybridized carbon atoms, and

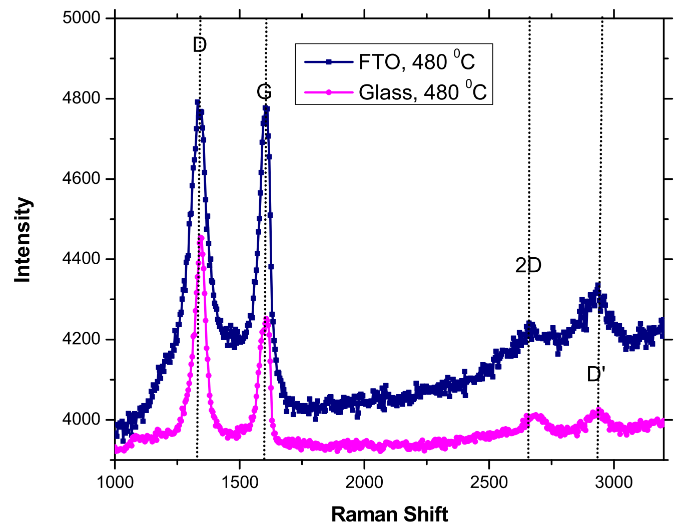

Fig. 4. Raman spectra of VGNs grown on Glass/FTO substrates at 480 °C.

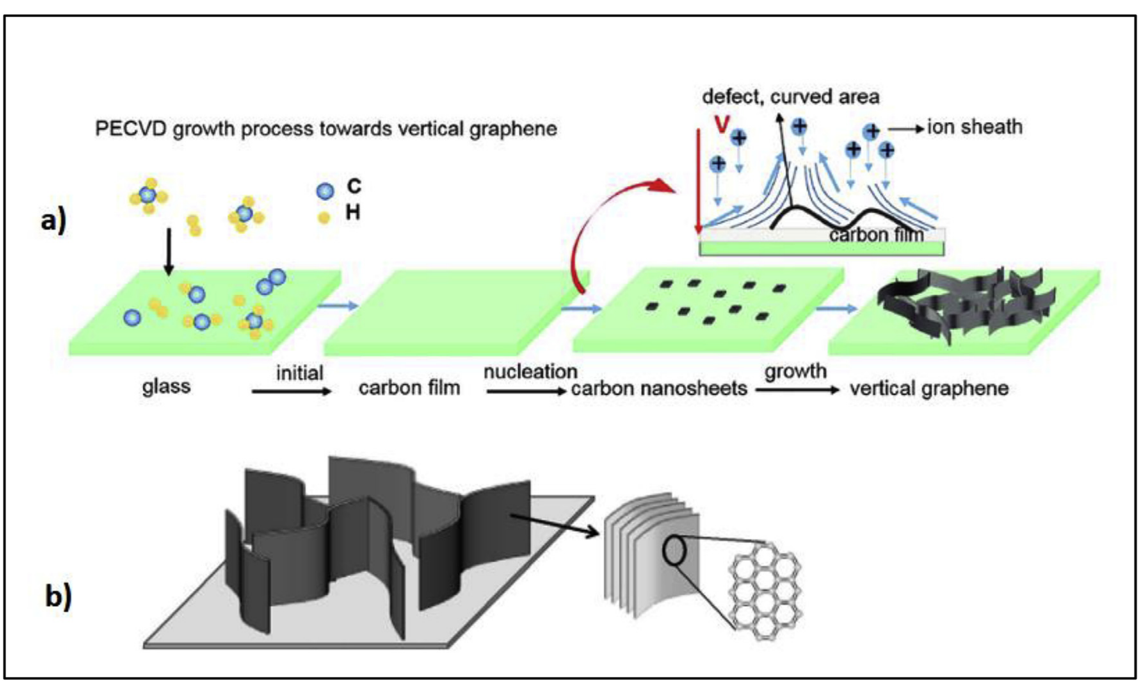

Fig. 3. Schematic represantation of graphene nanowalls formation.

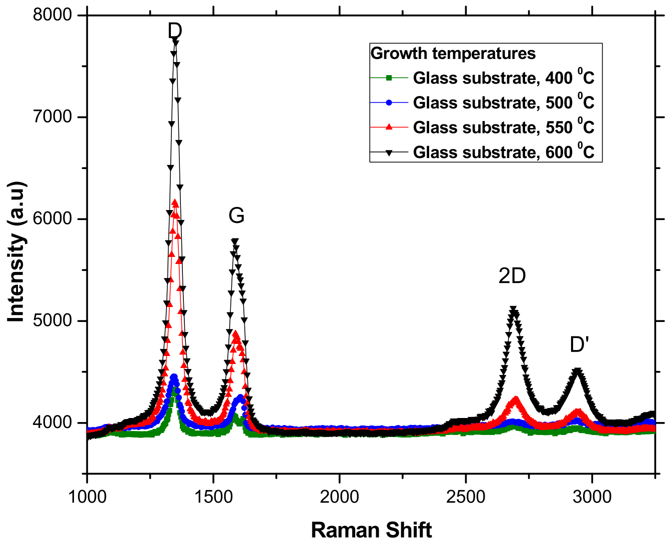

Fig. 5. Raman spectra of VGNs obtained at various temperatures on Glass substrates.

hence the number of defects in the VGN structure increases. In Figs. 4 and 5, it is clear that the D peak is more dominant with the increase in temperature compared to the other peaks. Furthermore, the increase in growth temperature caused the I_{2D}/I_G ratio to increase from 0.15 to 0.59. The increase in this ratio normally indicates a decrease in the graphene layer. However, the optical transmittance analysis of VGNs does not confirm this. Because, with increasing temperature, the optical transmittance of VGNs is reduced. This means that VGNs have a thicker layer and therefore a greater number of layers. This can be explained as follows: It is attributed to the fact that the VGN structure obtained at increasing temperature by the PECVD technique not only grows horizontally (graphitic) but also vertically as compared to 2D graphene. Although the number of horizontally oriented layers decreases with increasing temperature, the number of nanowalls growing in the vertical direction increases. Therefore, the VGNs obtained with increasing temperature are considered to have lower optical transmittance.

The full width at half maximum (FWHM) values of the D, G and 2D bands decreases depending on the growth temperature, and these values are presented in Table 1. It is understood that the growth temperature has an critical role on the peak positions and peak intensities of all characteristic peaks. The peak position of the D peak was represented by a sharp peak at approximately 1348 cm^{-1} for almost all VGNs. The other characteristic peak, the G peak, was determined to have relatively significant shifts and the G peak positions were determined as 1591 cm^{-1}, 1592 cm^{-1}, 1599 cm^{-1} and 1579 cm^{-1} with increasing temperature, respectively. The 2D peak associated with graphene quality was 2693 cm^{-1}, 2694 cm^{-1}, 2684 cm^{-1} and 2687 cm^{-1}, respectively, with increasing growth temperature. In order to determine the quality of graphene structures for the characteristic peaks of VGNs, the determined FWHM values are in good agreement with the literature. The detected FWHM values for G peak were 59.5 cm^{-1}, 51.1 cm^{-1}, 61.3cm^{-1} and 65.9 cm^{-1} with increasing growth temperature, respectively. For the VGNs obtained using the PECVD technique, the G peak FWHM values reported in the literature are in the range of 22.5 cm^{-1}–77.0 cm^{-1} [60–63], which indicates similar results to our study.

3.3. Morphological characteristic of VGN

SEM images of VGNs prepared at various growth temperatures (400^{0}C-600 °C) on Glass/FTO substrates were presented in Figs. 6 and 7. It is understood from these images that the growth temperature is an important factor for obtaining graphene nanostructures. At relatively low temperatures of 400 °C, a relatively weak 3D graphene film was formed. These results are consistent with the 2D peak density obtained from the Raman spectrum. When the growth temperature is not high enough, the concentration of carbon-based radicals formed by the thermal decomposition of CH4, which is used as the precursor, is low, resulting in a low growth rate of VGNs [64]. With increasing temperature, VGN nanowalls began to become more pronounced and a 3D nanowall structure is obtained when the growth temperature of 600 °C was reached. This can be explained by the increase in the concentration and kinetic energy of the carbon containing radicals at this temperature [64]. The graphene structures, which first formed as nano islands with the increase in temperature, then transform into well-aligned VGN nanowall structure with the temperature increasing further. These VGNs obtained at 600 °C exhibit more uniform and more random morphology than those obtained at low growth temperatures. SEM images at different magnifications for the VGN produced at 600 °C were taken and shown in Fig. 7(a–d). From these images, the homogeneous structure of VGN and the nanowalls thickness are more clearly seen. Considering the critical operating temperature for glass of 620 °C, the growth temperature of these nanowalls at 600 °C is a significant critical temperature value. For FTO, which is another substrate material, although the nanowwall structure has not yet clearly begun to occur at this temperature, the growth is more pronounced and more homogeneous compared to the VGN that is grown on glass substrate at the same temperature. The growth temperature determined for FTO is preferred because it is close to the critical operating temperature of FTO. Homogeneous morphologies of VGNs were also confirmed by Raman mapping and the spectrum for VGN1 was presented in Fig. 8. Raman mapping images of VGN1 were examined separately for all characteristic peaks. In this technique, all peaks for the whole film surfaces are scanned separately. Therefore, the characteristic of the structure occurring at all surfaces is determined. The Raman mapping of the D, G and D peaks shows that they exist homogeneously on all surfaces. In fact, there is a simple relationship between Raman mapping and Raman analysis. Fig. 8 shows that the number of counts determined for D, G and 2D peaks is related to the intensity of the peaks determined in Figure 5. As a result, homogeneous morphology and significant peaks of the graphene films were examined by Raman mapping.

3.4. Optical and electrical properties of VGNs

Fig. 9 shows the optical transmittance for the VGNs obtained on the Glass/FTO substrates. The optical transmittance measured for VGNs at 550 nm ranges from 50% to 95% depending on the growth temperature. Although these values are not as high as that of a single-layer graphene obtained by the CVD technique (95–97%), they are still comparable with the multi-layer graphene films obtained using these technique (60–90%) [65]. Similarly, I–V characteristics of VGNs were

Table 1
The intensities of characteristic peaks determined for VGNs, FWHM values of these peaks and its ratios according to each other.

Sample	$I_{D\ (a.u)}$	$I_{G(a.u)}$	$I_{2D(a.u)}$	2D FWHM(cm^{-1})	G FWHM(cm^{-1})	$I_{2D/IG}$	$I_{D/IG}$
VGN1	3541	1755	1048	101.2	65.9	0.59	2.01
VGN2	2061	918	266	102.5	61.3	0.29	2.24
VGN3	461	308	45	104.2	51.1	0.15	1.49
VGN4	410	157	52	82.1	59.4	0.33	2.61

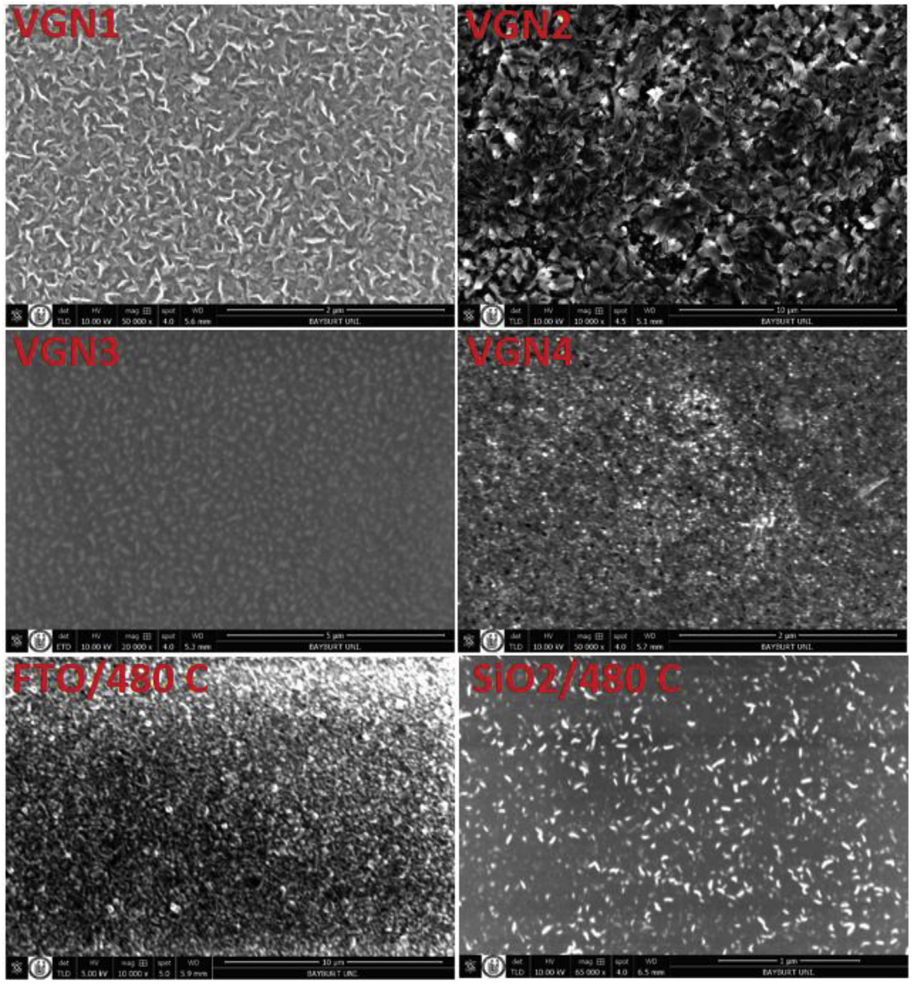

Fig. 6. SEM images of VGNs grown at various temperatures on Glass/FTO substrates.

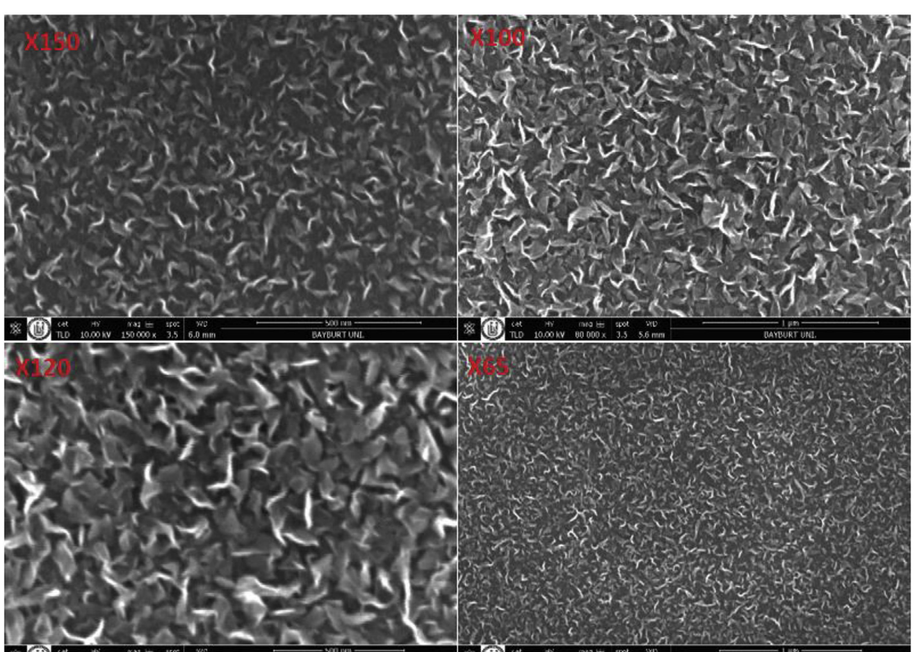

Fig. 7. SEM images taken at various magnification rates for VGN 1.

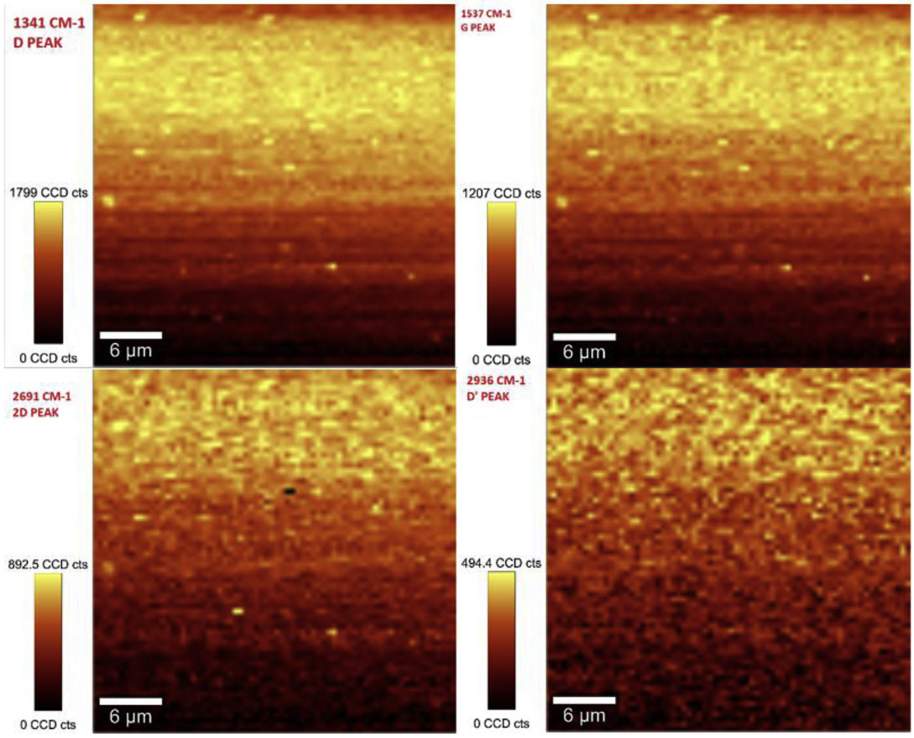

Fig. 8. Raman mapping of VGN1 obtained at 600 °C.

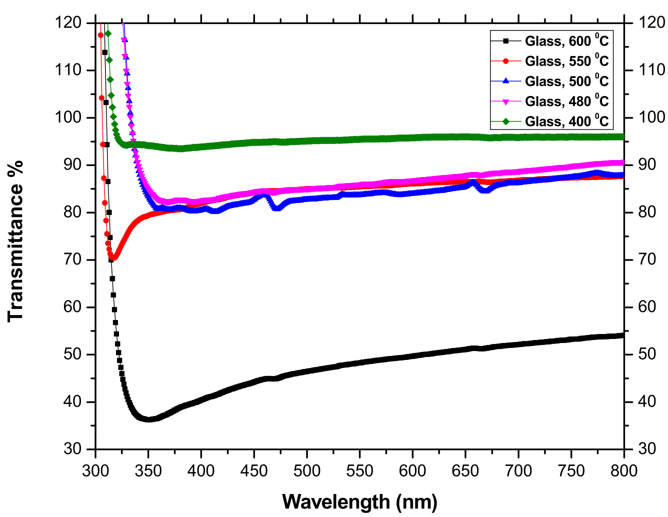

Fig. 9. Transmittance spectra of VGNs.

analyzed using four probe methods. The detected sheet resistances are similar and compatible with those reported in the literature [51,66]. The sheet resistance of the VGNs changed significantly depending on the growth temperature, ie the VGN nanowall morphology. This value linearly decreased from 8.34 kohm/sqr to 5.94 kohm/sqr depending on the growth temperature. The most noteworthy case was detected for FTO with untreated sheet resistance of 32 Ω/sqr and it was determined as 74.3 Ω/sqr after the treatment. The most important factor that draws attention here is the I_D/I_G ratio determined in the Raman spectra. For FTO, this ratio is approximately 1 (Fig. 4) and it is considered to be the most important factor affecting the sheet resistance.

4. Conclusion

In this study, VGN nanowalls were successfully produced by using PECVD technique on substrates such as Glass/FTO at relatively low temperatures. The optical transmittance of VGN nanowalls changed significantly depending on the growth temperature. The optical transmittance of VGN nanowalls decreased from 95% to 50% depending on the increasing growth temperature. The VGN obtained at a growth temperature of 600 °C was found to be more homogeneous and nanowalls morphology was more clear than others. The base temperature was determined to be about 400 °C to produce 3D graphene. Considering the D, G and 2D characteristic peaks determined by Raman analysis, it was found that the highest quality 3D graphene production was possible by increasing the growth temperature. Raman mapping showed that all VGNs had homogeneous morphology, meaning that vertical orientation growth occured not only on specific parts of the substrate but its all surfaces . It is thought that 3D graphene directly produced on the substrates such as FTO, which is a technological material, can be an alternative product to other 2D graphene commonly used in possible device applications such as solar cell, supercapasitor and biosensor.

Acknowledgements

This study is dedicated to my father, Ilyas BAYRAM, who supported me throughout my academic life. I will always pray for you. The author is grateful to NANOVAK company (Ankara, TURKEY) for all kinds of technical support.

References

[1] A.K. Geim, K.S. Novoselov, The rise of graphene, Nat. Mater. 6 (2007) 183.
[2] K.S. Kim, et al., Large-scale pattern growth of graphene films for stretchable transparent electrodes, Nature 457 (2009) 706.
[3] Y.-M. Lin, et al., 100-GHz transistors from wafer-scale epitaxial graphene, Science 327 (5966) (2010) p. 662-662.
[4] F. Schedin, et al., Detection of individual gas molecules adsorbed on graphene, Nat. Mater. 6 (2007) 652.
[5] X. Yang, et al., Liquid-mediated dense integration of graphene materials for compact capacitive energy storage, Science 341 (6145) (2013) 534–537.
[6] Y. Zhang, et al., Recent applications of graphene in dye-sensitized solar cells, Curr. Opin. Colloid Interface Sci. 20 (5–6) (2015) 406–415.
[7] Y. Zhang, et al., Recent applications of graphene in dye-sensitized solar cells, Curr.

Opin. Colloid Interface Sci. 20 (5) (2015) 406–415.
[8] X. Du, et al., Approaching ballistic transport in suspended graphene, Nat. Nanotechnol. 3 (8) (2008) 491.
[9] S. Unarunotai, et al., Conjugated carbon monolayer membranes: methods for synthesis and integration, Adv. Mater. 22 (10) (2010) 1072–1077.
[10] A. Peigney, et al., Specific surface area of carbon nanotubes and bundles of carbon nanotubes, Carbon 39 (4) (2001) 507–514.
[11] R.R. Nair, et al., Fine structure constant defines visual transparency of graphene, Science 320 (5881) (2008) p. 1308-1308.
[12] J. Du, et al., Hierarchically ordered macro− mesoporous TiO2− graphene composite films: improved mass transfer, reduced charge recombination, and their enhanced photocatalytic activities, ACS Nano 5 (1) (2010) 590–596.
[13] L.J. Brennan, et al., Carbon nanomaterials for dye-sensitized solar cell applications: a bright future, Adv. Energy Mater. 1 (4) (2011) 472–485.
[14] D. Chen, et al., Graphene and its derivatives for the development of solar cells, photoelectrochemical, and photocatalytic applications, Energy Environ. Sci. 6 (5) (2013) 1362–1387.
[15] L. Kavan, J.H. Yum, M. Graetzel, Application of graphene-based nanostructures in dye-sensitized solar cells, Phys. Status Solidi 250 (12) (2013) 2643–2648.
[16] J.D. Roy-Mayhew, I.A. Aksay, Graphene materials and their use in dye-sensitized solar cells, Chem. Rev. 114 (12) (2014) 6323–6348.
[17] L. Kavan, et al., Graphene nanoplatelet cathode for Co (III)/(II) mediated dye-sensitized solar cells, ACS Nano 5 (11) (2011) 9171–9178.
[18] L. Kavan, J.-H. Yum, M. Gra¨tzel, Graphene nanoplatelets outperforming platinum as the electrocatalyst in co-bipyridine-mediated dye-sensitized solar cells, Nano Lett. 11 (12) (2011) 5501–5506.
[19] J.D. Roy-Mayhew, et al., Functionalized graphene as a catalytic counter electrode in dye-sensitized solar cells, ACS Nano 4 (10) (2010) 6203–6211.
[20] X. Wang, L. Zhi, K. Müllen, Transparent, conductive graphene electrodes for dye-sensitized solar cells, Nano Lett. 8 (1) (2008) 323–327.
[21] H. Wang, Y.H. Hu, Graphene as a counter electrode material for dye-sensitized solar cells, Energy Environ. Sci. 5 (8) (2012) 8182–8188.
[22] T. Cohen-Karni, et al., Graphene and nanowire transistors for cellular interfaces and electrical recording, Nano Lett. 10 (3) (2010) 1098–1102.
[23] Q. He, et al., Centimeter-long and large-scale micropatterns of reduced graphene oxide films: fabrication and sensing applications, ACS Nano 4 (6) (2010) 3201–3208.
[24] T. Kuila, et al., Recent advances in graphene-based biosensors, Biosens. Bioelectron. 26 (12) (2011) 4637–4648.
[25] M.S. Mannoor, et al., Graphene-based wireless bacteria detection on tooth enamel, Nat. Commun. 3 (2012) 763.
[26] S. Mao, et al., Specific protein detection using thermally reduced graphene oxide sheet decorated with gold nanoparticle-antibody conjugates, Adv. Mater. 22 (32) (2010) 3521–3526.
[27] Y. Ohno, K. Maehashi, K. Matsumoto, Label-free biosensors based on aptamer-modified graphene field-effect transistors, J. Am. Chem. Soc. 132 (51) (2010) 18012–18013.
[28] W. Yang, et al., Carbon nanomaterials in biosensors: should you use nanotubes or graphene? Angew. Chem. Int. Ed. 49 (12) (2010) 2114–2138.
[29] Y. Zhang, et al., One-pot green synthesis of Ag nanoparticles-graphene nanocomposites and their applications in SERS, H 2 O 2, and glucose sensing, RSC Adv. 2 (2) (2012) 538–545.
[30] Y. Dong, et al., Graphene quantum dot as a green and facile sensor for free chlorine in drinking water, Anal. Chem. 84 (19) (2012) 8378–8382.
[31] G. Lu, et al., Toward practical gas sensing with highly reduced graphene oxide: a new signal processing method to circumvent run-to-run and device-to-device variations, ACS Nano 5 (2) (2011) 1154–1164.
[32] S. Mao, et al., Tuning gas-sensing properties of reduced graphene oxide using tin oxide nanocrystals, J. Mater. Chem. 22 (22) (2012) 11009–11013.
[33] F. Yavari, et al., High sensitivity gas detection using a macroscopic three-dimensional graphene foam network, Sci. Rep. 1 (2011) 166.
[34] J. Sun, et al., Direct chemical vapor deposition-derived graphene glasses targeting wide ranged applications, Nano Lett. 15 (9) (2015) 5846–5854.
[35] J. Chen, Z. Bo, G. Lu, Vertically-Oriented Graphene vol. 10, Springer International Publishing Switzerland, 2015 p. 978-3.
[36] D. Seo, et al., Vertical graphene gas-and bio-sensors via catalyst-free, reactive plasma reforming of natural honey, Carbon 60 (2013) 221–228.
[37] M. Cai, et al., Fast response, vertically oriented graphene nanosheet electric double layer capacitors synthesized from C2H2, ACS Nano 8 (6) (2014) 5873–5882.
[38] B. Ouyang, et al., Green synthesis of vertical graphene nanosheets and their application in high-performance supercapacitors, RSC Adv. 6 (28) (2016) 23968–23973.
[39] Y. Ma, et al., Copper-Assisted direct growth of vertical graphene nanosheets on glass substrates by low-temperature plasma-enhanced chemical vapour deposition process, Nanoscale Res. Lett. 10 (1) (2015) 308.
[40] D.H. Seo, et al., Plasma break-down and Re-build: same functional vertical graphenes from diverse natural precursors, Adv. Mater. 25 (39) (2013) 5638–5642.
[41] J.R. Miller, R. Outlaw, B. Holloway, Graphene double-layer capacitor with ac line-filtering performance, Science 329 (5999) (2010) 1637–1639.
[42] C. Yang, et al., Direct PECVD growth of vertically erected graphene walls on dielectric substrates as excellent multifunctional electrodes, J. Mater. Chem. 1 (3) (2013) 770–775.
[43] J. Wang, et al., Synthesis of carbon nanosheets by inductively coupled radio-frequency plasma enhanced chemical vapor deposition, Carbon 42 (14) (2004) 2867–2872.
[44] Z. Bo, et al., Vertically oriented graphene bridging active-layer/current-collector interface for ultrahigh rate supercapacitors, Adv. Mater. 25 (40) (2013) 5799–5806.
[45] C. Zhu, et al., All metal nitrides solid-state asymmetric supercapacitors, Adv. Mater. 27 (31) (2015) 4566–4571.
[46] D.H. Seo, et al., Synergistic fusion of vertical graphene nanosheets and carbon nanotubes for high-performance supercapacitor electrodes, ChemSusChem 7 (8) (2014) 2317–2324.
[47] T.-C. Hung, C.-F. Chen, W.-T. Whang, Deposition of carbon nanowall flowers on two-dimensional sheet for electrochemical capacitor application, Electrochem. Solid State Lett. 12 (6) (2009) K41–K44.
[48] X. Cao, Z. Yin, H. Zhang, Three-dimensional graphene materials: preparation, structures and application in supercapacitors, Energy Environ. Sci. 7 (6) (2014) 1850–1865.
[49] S. Pekdemir, M.S. Onses, M. Hancer, Low temperature growth of graphene using inductively-coupled plasma chemical vapor deposition, Surf. Coating. Technol. 309 (2017) 814–819.
[50] Z. Chen, et al., Direct CVD growth of graphene on traditional glass: methods and mechanisms, Adv. Mater. (2018) 1803639.
[51] L. Zhang, et al., Catalyst-free growth of nanographene films on various substrates, Nano Res. 4 (3) (2011) 315–321.
[52] Y.S. Kim, et al., Direct integration of polycrystalline graphene into light emitting diodes by plasma-assisted metal-catalyst-free synthesis, ACS Nano 8 (3) (2014) 2230–2236.
[53] O. Bayram, O. Simsek, Vertically oriented graphene nano-sheets grown by plasma enhanced chemical vapor deposition technique at low temperature, Ceram. Int. 45 (11) (2019) 13664–13670.
[54] H. Ci, et al., 6-inch uniform vertically-oriented graphene on soda-lime glass for photothermal applications, Nano Res. 11 (6) (2018) 3106–3115.
[55] M. Hiramatsu, H. Kondo, M. Hori, Graphene nanowalls, New Progress on Graphene Research, IntechOpen, 2013.
[56] D.H. Seo, S. Kumar, K. Ostrikov, Control of morphology and electrical properties of self-organized graphenes in a plasma, Carbon 49 (13) (2011) 4331–4339.
[57] Z.L. Tsakadze, et al., Plasma-assisted self-organized growth of uniform carbon nanocone arrays, Carbon 45 (10) (2007) 2022–2030.
[58] L.M. Malard, et al., Raman spectroscopy in graphene, Phys. Rep. 473 (5) (2009) 51–87.
[59] Q. Yang, et al., Vertically-oriented graphene nanowalls: growth and application in Li-ion batteries, Diam. Relat. Mater. 91 (2019) 54–63.
[60] K. Teii, et al., Synthesis and electrical characterization of n-type carbon nanowalls, J. Appl. Phys. 106 (8) (2009) 084303.
[61] Z. Bo, et al., Understanding growth of carbon nanowalls at atmospheric pressure using normal glow discharge plasma-enhanced chemical vapor deposition, Carbon 49 (6) (2011) 1849–1858.
[62] N. Soin, et al., Microstructural and electrochemical properties of vertically aligned few layered graphene (FLG) nanoflakes and their application in methanol oxidation, Mater. Chem. Phys. 129 (3) (2011) 1051–1057.
[63] N. Soin, et al., Exploring the fundamental effects of deposition time on the microstructure of graphene nanoflakes by Raman scattering and X-ray diffraction, CrystEngComm 13 (1) (2011) 312–318.
[64] X. Guo, et al., Vertical graphene nanosheets synthesized by thermal chemical vapor deposition and the field emission properties, J. Phys. D Appl. Phys. 49 (38) (2016) 385301.
[65] M. Othman, et al., Low-temperature plasma-enhanced chemical vapour deposition of transfer-free graphene thin films, Mater. Lett. 158 (2015) 436–438.
[66] H. Medina, et al., Metal-free growth of nanographene on silicon oxides for transparent conducting applications, Adv. Funct. Mater. 22 (10) (2012) 2123–2128.